Ions in Crystals: The Topology of the Electron Density in Ionic Materials. 4. The Danburite ($CaB_2Si_2O_8$) Case and the Occurrence of Oxide−Oxide Bond Paths in Crystals

Victor Luaña, Aurora Costales,* Paula Mori-Sánchez, and A. Martín Pendás

Departamento de Química Física y Analítica, Facultad de Química, Universidad de Oviedo, 33006-Oviedo, Spain

Received: November 7, 2002; In Final Form: March 4, 2003

We have obtained the electron density of danburite by means of *ab initio* Perturbed Ion (aiPI) quantum mechanical calculations and fully characterized its topological features, as required for the analysis of crystal bonding in the light of Bader's atoms in molecules (AIM) theory. Our theoretical results are compared with the experimental determination by Downs and Swope (*J. Phys. Chem.* **1992**, *96*, 4834). Each B and Si ion is bound to its four nearest oxide ions in a deformed tetrahedral disposition, whereas Ca is bonded to seven oxide ions. What makes this mineral most interesting is a rich collection of O−O long-distance bond paths. Their existence is examined in several crystalline oxides and gas phase molecules. The occurrence of bond paths is not simply due to the distance between atoms but rather is a consequence of the molecular and crystal geometry. It is shown that the electron density at the bond critical point decreases exponentially as the distance between atoms increases. This relationship groups together molecules and crystals, neutral oxygen and oxide ions, with bonds from 1.2 to 3.2 Å, both covalent and ionic.

I. Introduction

From the first days of quantum mechanics, the chemical bond in molecules and solids has been interpreted in terms of concepts produced by the simplest MO-LCAO (molecular orbitals made as linear combinations of atomic orbitals) approximation. Whereas this approach has been a fruitful source of chemical insight, it is well-known that many LCAO bonding concepts dissipate when large sets of basis functions (atomic or otherwise) are used and even more when the molecular wave function is systematically improved in configuration interaction (CI) calculations. Furthermore, new powerful theoretical techniques generate wave functions that can explain experimental data without resort to the indirect approach of referring to molecular orbitals or the LCAO approximation. This situation has led several research groups to develop and use new approaches to the concept of chemical bonding, extracting the chemical information from the wave function itself or from properties derived from it, such as the electron density. This provides a sound definition for the chemical bonding concepts, since they become physical properties of the state of the system, on equal footing with other observables such as the energy.

One of the most successful approches is the work by Bader and collaborators,[1−6] and it is usually known as the quantum theory of atoms in molecules (AIM). The AIM theory is founded on the Lagrangian formulation of quantum mechanics[7] and, particularly, on Schwinger's stationary action principle.[8] Through the generalization of this formulation to open subsystems (i.e. systems extending in a limited region of space), Bader was able to demonstrate that quantum mechanical laws do not apply locally to arbitrary regions of the molecular systems. They apply if and only if the regions are chosen according to the criterion that the flux of the electron density through their limiting surfaces is null, $\vec{\nabla}\rho\cdot\vec{n} = 0$. In this case, each quantum mechanical law is locally satisfied, and each observable property is locally well defined. Accordingly, the atoms and functional groups of chemistry can be identified with regions of space whose properties are well defined, which additively contribute to the total properties of molecules and which bind together, providing an unequivocal description of molecular structure.

Although a review of all AIM studies done lies outside of the purpose of this work, we should mention that the extension of AIM concepts to crystalline solids has been analyzed in refs 9−11. High-quality experimental densities of minerals,[12−20] covalent,[21] metallic,[22] and molecular crystals[23−27] have been analyzed in terms of AIM concepts. In addition, theoretical calculations on simple metals,[28−30] alloys and intermetallic phases,[31−40] molecular,[10,30,41,42] covalent, and ionic crystals,[11,20,21,30,43−49] as well as impurity centers and defects[50−53] have been reported.

The electron density of danburite ($CaB_2Si_2O_8$), a naturally occurring borosilicate, has been determined by Downs and Swope from X-ray diffraction experiments[14] and analyzed in light of the AIM theory. Even though the experimental noise precluded Downs and Swope from obtaining all topological features of the crystal, their data provide an excellent test for theoretical calculations of the crystal wave function and for ideas regarding bonding on ionic crystals.

Two of the results from Downs and Swope's article are particularly appealing. First, danburite is shown to be an ionic crystal, all Ca−O, B−O, and Si−O bonds presenting a local depletion of electron density ($\nabla^2\rho_b > 0$) at the bond critical point. Second, the oxide ions are highly polarized and unspherical, extending 0.937 ± 0.003 Å in the Si−O bond directions, 0.992 ± 0.015 Å in the B−O direction, and 1.246 ± 0.023 Å along the Ca−O bond path.[54] This observation supports Pauling's argument that the bonding radius of an atom should be inversely proportional to the electronegativity of the atom to which is bonded. It can also be viewed as an evidence of the polyhedral shape of the ionic basins in crystals.[11]

* E-mail: yoyi@carbono.quimica.uniovi.es.

10.1021/jp022374f CCC: $25.00
Published on Web 05/01/2003

On the other hand, recent works in ionic crystals,[11,46] hydrocarbons with large substituent functional groups,[55−57] and van der Waals aggregates[58] have shown the occurrence, in many instances, of long-range, low-density bonds. Some authors have raised doubts about whether these topological bonds should be considered as true chemical bonds or rather viewed as mathematical artifacts.[55−57,59] Danburite is a very interesting system in relation to this problem, because it has five nonequivalent oxide positions, each having a very different local environment. Unfortunately, the occurrence of O−O bonds in danburite has not been experimentally examined.

Our main objective in this work is to produce a complete characterization of all the topological features of danburite's electron density. To this end, we have used the techniques previously developed and applied to alkali halides and halide perovskites.[11,46] These techniques are briefly described in section II. The topological properties of the electron density are presented and discussed in section III. Section IV examines the shape and properties of atoms in the crystal. Finally, the occurrence of O−O bonds is addressed in section V.

II. Theoretical Procedure

As in previous works,[11,46,47] the crystal wave function has been obtained by means of *ab initio* Perturbed Ion (aiPI)[60−62] calculations at the experimental geometry.[14] The aiPI method is a localized Hartree−Fock (HF) scheme[60,63,64] that has been extensively used to describe accurately the electronic structure, geometry, and thermodynamical properties of ionic and partly ionic pure and defective solids.[60,65−71] The multi-ζ exponential basis sets by Clementi and Roetti[72] for Ca^{2+}, B^{3+}, Si^{4+}, and O^{-} have been used in the present aiPI calculations.

In addition, Dovesi's et al. CRYSTAL98[73] code has been used to obtain HF-LCAO (linear combination of atomic orbitals) electron densities on a collection of test crystals that provide independent validation of our aiPI results on danburite. Common practice techniques[73] have been used to truncate and adapt to the crystals double- or triple-ζ valence (DZV or TZV) gaussian molecular basis sets, as described in ref 30.

It is worth mentioning that aiPI and CRYSTAL98 wave functions do complement each other nicely for the purposes of this work. Whereas CRYSTAL98 provides a reliable description of the bond critical points with a significant electron density accumulation, aiPI works best at providing a good description of the low-density regions and producing stable trends across families of compounds.

The electron densities obtained from the aiPI or CRYSTAL98 calculations has been the input to the Critic program,[74] a code that automatically searches for all the independent critical points in a crystal lattice. Two different search methods have been used. The first method, previously described in ref 11, is based on the recursive division of the irreducible wedge of the Wigner−Seitz polyhedron of the Bravais lattice and the minimization of $|\vec{\nabla}\rho|$ within the edges, surfaces, and interiors of the resulting tetrahedra. Even though this method works nicely in many simple crystals, it failed to find many critical points of danburite.

Accordingly, we have turned to a brute force method that happened to be quite robust at getting all critical points of danburite. The method starts by recursively dividing the crystal cell into tetrahedra up to a recursion level previously fixed (usually 4 or 5 levels, which represents 425 or 1705 tetrahedra). Then, a Newton−Raphson search is done, starting from the baricenter of each tetrahedra, to find the solutions of the equation $\vec{\nabla}\rho = \vec{0}$. The value of the gradient at each end point must be checked to be below an appropriate threshold, as the Newton−Raphson search is not guaranteed to converge on a critical point. Most critical points, on the other hand, are reached many times, so the last step of the algorithm is replicating the points by symmetry and deleting the repeated ones. The final set must fulfill the Morse relationships:

$$n - b + r - c = 0 \tag{1}$$

and

$$n \geq 1, \quad b \geq 3, \quad r \geq 3, \quad c \geq 1 \tag{2}$$

where n, b, r, and c are the total number of nuclear, bond, ring, and cage critical points of the electron density in the crystal cell, respectively.

On the other hand, we have also analyzed the occurrence of Si−O, Ca−O, B−O, and O−O bonds on several small molecules to the end of comparing with the results on danburite. Those calculations have been done with GAMESS[75] using triple-ζ valence plus diffuse and polarization functions at the Hartree−Fock level. The topological analysis of the GAMESS wave function has been done with the AIMPAC package.[76]

III. Topological Properties of the Electron Density in Danburite

Danburite crystallizes in the orthorhombic system with space group *Pnam* and lattice parameters $a = 8.0456(7)$, $b = 8.7629(4)$, and $c = 7.7341(7)$ Å at 300 K.[14] The location and properties of all theoretical bond critical points have been collected in Table 1 and compared with the available experimental values. Nuclear, ring, and cage critical points have also been determined and are available upon request. We have found $n = 52$, $b = 164$, $r = 136$, and $c = 24$, which fulfill the Morse relations and can be compared with the experimentally known set of $n = 52$ and $b = 92$.[14]

Up to 23 different bond critical points have been found in danburite's theoretical density. In the AIM framework, whenever there exists a bond critical point between two atoms, these atoms are considered to be bonded, and the gradient line connecting both nuclei and the bond critical point is referred to as the *bond path* or simply the *bond* between the two atoms. Each Si and B is bonded to four oxide ions in a distorted tetrahedral configuration. Ca, on the other hand, is bonded to seven oxide ions in a configuration similar to a distorted octahedron with an extra bond appearing where an octahedron edge should be. This bonding pattern is the same as that found experimentally, and in fact, there is an excellent agreement between the theoretical and the experimental positions of the M−O bond critical points[14] (see Table 1). There is also agreement with the value of the density and the Laplacian at the Ca−O bond critical points. However, the aiPI theoretical density at the Si−O bond critical point is only about 65% of the experimental value, and 45% for the B−O bond. The aiPI values for the Laplacians are also significantly larger than the experimental values, even taking into account an estimated experimental error[14] of the order of 25%. This discrepancy on the B−O and Si−O bond critical properties is mostly due to the approximations incorporated within the aiPI technique, in particular the enforced radial symmetry of the electron density contributed by each ion. This approximation is expected to become poorer as the covalent accumulation of electron density increases. On the contrary, the use of a saturated exponential basis set is expected to work best on the representation of mostly ionic bonding, in addition to providing stability of the bond properties across families of compounds.

TABLE 1: Theoretical (First Row) and Experimental (Second Row When Available) Bond Critical Points of Danburite[a]

Wyckoff	bond	x	y	z	R_1[b]	R_2[b]	ρ_b	$\nabla^2\rho_b$	$\lambda_3(b)$	ϵ[c]
8d	Ca−O1	0.29145	0.07125	0.12505	1.2285	1.2713	0.1604	3.8317	5.2396	6.90
		0.2880	0.0733	0.1228			0.142(3)	3.23		
8d	Ca−O2	0.37890	0.97270	0.35269	1.2089	1.2460	0.1817	4.2908	5.9416	4.83
		0.3791	0.9709	0.3553			0.166(3)	3.73		
8d	Ca−O3	0.39243	0.19332	0.16563	1.2150	1.2526	0.1733	4.1484	5.7394	1.89
		0.3927	0.1949	0.1622			0.161(3)	3.57		
4c	Ca−O5	0.53289	0.07428	0.25000	1.1856	1.2153	0.2115	4.8858	6.8848	0.75
		0.5368	0.0736	0.25			0.184(5)	4.14		
8d	B−O1	0.22548	0.96781	0.94593	0.4836	0.9955	0.4832	26.7631	36.7152	1.28
		0.2205	0.9675	0.9406			0.93(6)	11.85		
8d	B−O2	0.21572	0.40190	0.03958	0.4886	1.0117	0.4525	24.9145	33.8588	1.99
		0.29139	0.3989	0.0438			0.99(3)	6.04		
8d	B−O3	0.30509	0.38463	0.07901	0.4798	0.9834	0.5092	28.4002	39.1935	1.52
		0.3052	0.3850	0.0784			1.13(5)	7.63		
8d	B−O5	0.23417	0.42207	0.13531	0.4778	0.9763	0.5265	29.1554	40.3686	1.18
		0.2432	0.4202	0.1358			1.15(5)	6.95		
8d	Si−O1	0.11201	0.14006	0.96627	0.6812	0.9375	0.6584	28.1712	39.6897	0.09
		0.1094	0.1385	0.9666			1.01(4)	17.56		
8d	Si−O2	0.8400	0.26499	0.94980	0.6825	0.9413	0.6484	27.7733	39.0528	0.23
		0.0856	0.2639	0.9515			0.95(3)	17.16		
8d	Si−O3	0.48862	0.30996	0.00066	0.6799	0.9351	0.6675	28.6467	40.3599	0.22
		0.4883	0.3129	−0.0009			0.95(4)	19.46		
8d	Si−O4	0.47498	0.68039	0.36237	0.6806	0.9352	0.6626	28.3908	40.0015	0.06
		0.4725	0.6802	0.3617			0.94(4)	18.30		
8d	O2−O1	0.28288	0.96603	0.48110	1.1624	1.1619	0.3127	5.0472	7.6690	3.35
8d	O2−O5	0.15642	0.39682	0.39658	1.1874	1.1871	0.2766	4.5689	6.7971	6.19
8d	O3−O5	0.29124	0.37154	0.33725	1.2021	1.2029	0.2554	4.3665	6.3211	15.09
8d	O3−O1	0.35147	0.44016	0.04131	1.2098	1.2102	0.2455	4.2252	6.1018	13.11
8d	O3−O2	0.26303	0.34093	0.01918	1.2148	1.2157	0.2396	4.1421	5.9560	12.06
8d	O5−O1	0.24577	0.49408	0.12393	1.2380	1.2376	0.2172	3.9563	5.2931	44.55
4c	O3−O3	0.39731	0.31448	0.25000	1.3275	1.3275	0.1336	2.4896	3.4534	12.13
8d	O3−O1	0.70470	0.80852	0.96251	1.3962	1.3978	0.0937	1.7990	2.4525	10.33
4c	O2−O2	0.37717	0.87129	0.25000	1.6063	1.6063	0.0336	0.7379	0.8526	88.98
4b	O2−O2	0.50000	0.00000	0.50000	1.5958	1.5958	0.0333	0.7073	0.9109	3.52
4c	O5−O4	0.41326	0.12770	0.75000	1.9157	1.9206	0.0065	0.1564	0.1725	4.96

[a] Ionic radii (R_1 and R_2) are given in Å, bond densities (ρ_b) in e/Å^3, bond Laplacians and curvatures ($\nabla^2\rho_b$ and $\lambda_3(b)$) in e/Å^5, and ellipticities[c] (ϵ) in %. [b] We define the ionic radius as the distance between the bond critical point and each corresponding nucleus. [c] We define the ellipticity as $\epsilon = 1 - \lambda_2/\lambda_1$ rather than using Bader's definition ($\lambda_1/\lambda_2 - 1$). The advantage of our definition is that ϵ lies in the range [0, 1].

To provide an independent validation of our results, we have compared the aiPI and CRYSTAL98 electron densities for a representative collection of oxide crystals: ionic compounds such as MgO, ZnO, and CaO; polar crystals such as α-quartz, TiO_2 (both rutile and anatase phases), $AlBO_3$, and $CaTiO_3$; and even molecular compounds such as N_2O_4. The comparison shows that aiPI systematically underestimates the electron density accumulation in covalent and highly polar compounds. For instance, the ratio of aiPI to CRYSTAL98 ρ_b values is about 74−76% on the Si−O bond critical points and 50% on the B−O ones. The agreement is much better in the *more ionic* cases: 80−95% on Ca−O, 83% on Ti−O, or 87% on Zr−O. More important, the CRYSTAL98 and aiPI calculations agree qualitatively on the occurrence of O−O bonds such as those found on danburite and quantitatively on the O−O bond point properties.

Furthermore, we can gain additional understanding on the crystal bonding and the aiPI results by turning to examine the electron density of SiO, BO, and CaO diatomic molecules, as they provide a model of the electron density behavior when the interatomic distance changes. Table 2 presents the topological bond properties of the three molecules at their respective equilibrium distances. The calculations have been done with high-quality basis sets at the Hartree−Fock level, and we have checked that the bond properties do not change appreciably when correlation effects, up to a CI-SD level (configuration interaction including single and double excitations), are included. We can observe that bond lengths are consistently shorter in the molecule than in the crystal for the same pair of atoms,

TABLE 2: Equilibrium Geometry and Bond Topological Properties of Some Reference Molecules[a]

	state	R_{AB} (Å)	ρ_b (e/Å^3)	$\nabla^2\rho_b$ (e/Å^5)
SiO	$X^1\Sigma^+$	1.5097	1.268 53	35.7156
BO	$X^2\Sigma^+$	1.205	2.090 93	44.1469
CaO	$X^1\Sigma^+$	1.9426	0.689 47	14.0227

[a] The calculations have been done with GAMESS[75] at the Hartree−Fock level using a TZV+(3d1f) basis set. The topological analysis has been done with Bader's AIMPAC suite.[76]

with the electron density and its Laplacian at the bond critical points being much larger in the molecules.

To be able to compare molecular and crystal densities, we need to put them on the same distance scale. Accordingly, we have represented the bond density versus the interatomic distance for the reference molecules in Figure 1. The most important thing to observe is that ln ρ_b decreases linearly with the interatomic distance, R_{AB}, for a large range of distances that includes both the molecular equilibrium distance and the distances in danburite under normal pressure and temperature. The reason for this linear behavior is directly inherited from the properties of the radial electron density, $\rho(r)$, of the free atoms. Effectively, ln $\rho(r)$ decreases from the maximum cusp at the nucleus following linear steps, each step being related to one of the K, L, M, ... electron shells. Different linear steps, on the other hand, have different slopes, and they are separated by rather curved arms. Those linear regimes are found to be essentially conserved on many molecules that we have analyzed, both diatomic and polyatomic. It is quite interesting to notice

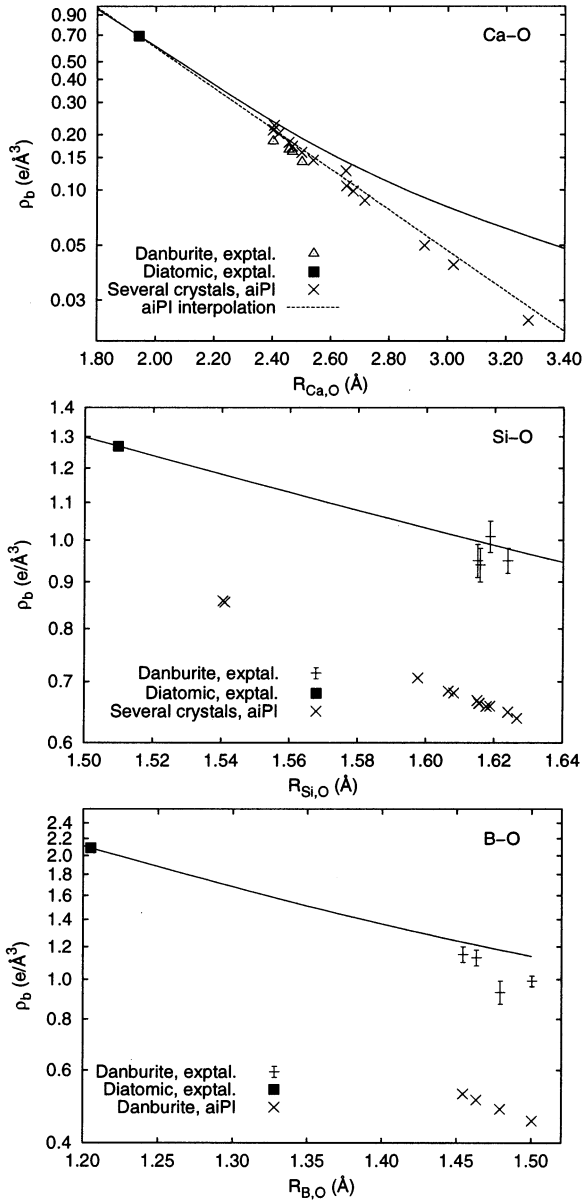

Figure 1. Electron density *versus* interatomic distance for the Ca−O, Si−O, and B−O bonds in danburite and the corresponding diatomic molecules. The solid lines correspond to the bond critical point densities (ρ_b) of the corresponding diatomic molecules for a range of internuclear distances. Notice the logarithmic scale for the density.

that ρ_b is a measurement of the bond strength, and it has been observed to correlate with the traditional bond order, n, as $n = \alpha\rho_b^{\beta}$ or $n = \alpha \exp(\beta\rho_b)$ (ref 4). We can then relate bond order and distance or, which is more striking, use a single and unified concept to deal with, say, the C−C bond on such molecules as C_2H_6, C_2H_4, C_6H_6, C_2H_2, and C_2.

Figure 1 shows that the molecular values of ρ_b correlate quite well with the experimental values on danburite when the same interatomic distances are considered. This result suggests that the molecular and crystalline regimes are manifestations in a different distance range of an unique universal regime. The experimental densities on the crystal show, on the other hand, significant error bars that could, perhaps, be reduced if the molecular results were used to refine the analysis of the X-ray diffraction data. The aiPI densities for the Ca−O bond agree with the molecular results. Even more, the aiPI bond densities obtained in a collection of crystals that includes several phases of $CaTiO_3$ and CaO, as well as danburite, predict exactly the

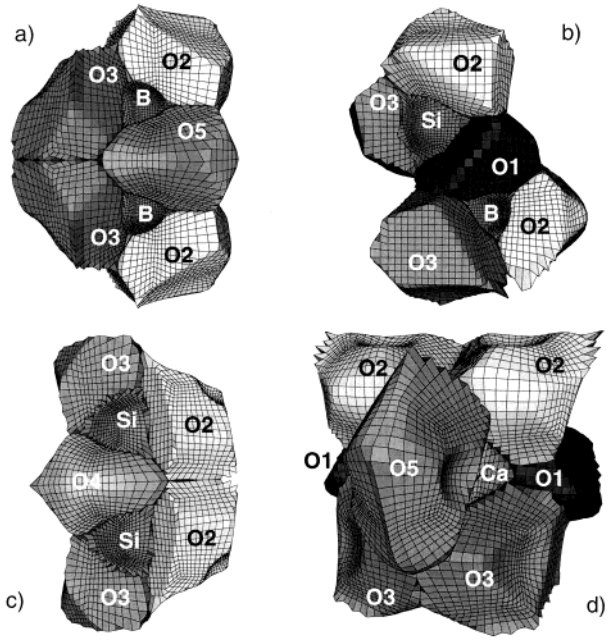

Figure 2. Atomic basins for the ions in danburite. From left to right, up to down: (a) Two BO_4^{5-} groups united by a O5 bridge. Each B is surrounded by O1 (subtracted to show the B basin), O2, O3, and O5 atoms. (b) An O1 basin acts as a bridge between the SiO_4^{4-} (up) and BO_4^{5-} tetrahedra (O4 and O5 have been subtracted around Si and B, respectively). (c) The SiO_4^{4-} tetrahedra are bridged by an O4 basin. Each Si edge in the Si basin extends in the space as a nearly bidimensional wing and is surrounded by O1 (subtracted to show the Si basin), O2, O3, and O4 atoms. (d) The Ca basin is heptacoordinated by two O2 basins (up), two O1 basins (middle), two O3 basins (down), and a single O5 basin (front). The figures have been created with Geomview.[78]

calculated molecular bond density when extrapolated to the molecular distance. The same extrapolation, however, predicts densities on the diatomic Si−O and B−O bonds that are about half of what should be expected from the diatomic molecule calculations, owing to the more covalent character of these diatomics.

It appears, from the above analysis, that the aiPI wave function underestimates the electron density in tetrahedral bonds, but it is satisfactory representing bonds from higher coordination environments. This conclusion is in accordance with the lack of multipolar contributions to the energy and wave function in the present aiPI calculations.[61,62] These difficulties should be overcome in the next *generalized Perturbed Ion* method,[77] which is presently being coded.

IV. Shape and Properties of Atoms

We can now turn to discuss the shape and properties of atoms in danburite. In a solid, we have shown[11] that the smallest proper quantum subsystems are the *primary bundles*. A primary bundle is the set of all points traversed by upward trajectories of the electron density gradient field that start at a given minimum and end at a given maximum. The collection of all bundles that have the same maximum as a common vertex forms the *attraction basin* for that particular maximum. The integration of appropriate functionals over the basin gives the atomic properties, which are well defined for any quantum mechanical observable, are additive to give the total property of the system, and are maximally transferable among systems up to the point that the basin shape is maintained.

The basin shapes of the ions in danburite are shown in Figure 2. Basins are topologically equivalent to polyhedra, in the sense

that they have faces, edges, and vertexes, and they satisfy Euler's relationship (faces − edges + vertexes = 2). Unlike polyhedra, however, basins tend to have rather curved edges and faces. Each face is the attraction surface of a bond critical point, edges are the attraction lines of a ring, and vertexes are minima of the electron density. Accordingly, ionic basins provide another way of looking at the crystal bonding.

Bonding in crystals is dominated by geometric factors. The existence of a bond path is not simply due to the distance between a particular pair of atoms, but it is rather the result of a complex balance among the basins of many neighbors. We have already observed that behavior on the rock-salt phase of alkali-halides and simple oxides (AX): the ratio among anion and cation topological radii (r_X and r_A, respectively) on the A−X bond path is an exact predictor of whether there is ($r_X/r_A >$ 1.15) or is not (<1.15) a X−X bond path.[47,48] Similar rules hold for the CsCl phase,[47,48] perovskites,[46] fluorites, and other prototypical crystalline structures.[49]

Danburite presents some striking examples of this balance principle. Whereas B, Si, Ca, and O1 ions are bonded to their nearest neighbors up to a given distance, the behavior of O2, O3, O4, and O5 ionic basins is quite different. O4 ions, for instance, being the bridge among two SiO_4 tetrahedra, are bonded to both Si ions at 3.083 Å and to an O5 ion placed quite far away (6.353 Å), even though there are 10 oxide ions and four B ions in the range 4.99−6.27 Å to which O4 ions are not bonded.

The most striking feature of ionic basins is, perhaps, their anisotropy and irregular shape, as we can appreciate in Figure 2. The distance from the nucleus to its basin's surface is quite different depending on the direction. In addition, basin shapes on danburite reflect the low symmetry of the ions within the crystal. We could conclude, naïvely, that when the ion shape is something completely different from a sphere, the classical notion of ionic radius is not compatible with Bader's AIM theory. However, our previous work has clearly shown us that the topological radii, defined as the distance from a nucleus to its bond critical points, can be compared to and have the predictive role of the empirical ionic radii.[47,48]

In agreement with this idea, the topological radii of cations show a very small variation among the different bonds in danburite: $r_B = 0.483 \pm 0.005$ Å, $r_{Si} = 0.681 \pm 0.001$ Å, and $r_{Ca} = 1.213 \pm 0.014$ Å. Oxide ions, on the contrary, present a wide range of values: 0.935−1.921 Å. Quite interestingly, the radii of oxide ions are more or less constant when bonded to a particular cation—$r_O(Si-O) = 0.937 \pm 0.003$, $r_O(B-O) = 0.989 \pm 0.015$, and $r_O(Ca-O) = 1.246 \pm 0.023$ Å—but show a large variability when bonded to other oxide ions: $r_O(O-O) = 1.33 \pm 0.23$ Å. The image of hard cations versus soft, polarizable anions is a natural conclusion from these results. This image is clearly compatible with the description of ionic crystals traditional since Pauling.[79]

Regarding the basin shapes as we can see in Figure 2, B and Si appear as slightly deformed tetrahedra, Ca is a heptahedron with bilateral symmetry, and the oxide basins have a very variable number of faces: 7 (O1), 8 (O2 and O3), 3 (O4), and 10 (O5). The basin of O4 is, in fact, one of the strangest we have found in studying many kinds of crystals. Each O4 ion is only bonded to two equivalent Si ions ($r_{O4}(Si-O4) = 0.935$ Å) and to a single O5 ion ($r_{O4}(O4-O5) = 1.921$ Å). Accordingly, the O4 basin, which must show bilateral symmetry, has only three faces with a very large curvature (see Figure 2).

The integration of appropriate functionals over the basins provides the properties of ions. Table 3 lists the basin volume and net charge of danburite's ions. As the integration is done numerically, it is relevant to indicate that the residual charge on the unit cell due to the integration errors is −0.018 *e*, and the absolute error in the cell volume is −0.125 Å^3, which represents a relative error of −0.023%. According to our calculations, the net charges of all ions are very close to their nominal oxidation states: $\mathcal{Q}_{Ca} = 1.9$, $\mathcal{Q}_B = 2.9$, $\mathcal{Q}_{Si} = 3.7$, and $\mathcal{Q}_O^{av} = -1.9$. Comparison with CRYSTAL98[73] calculations on simpler oxides[30] suggests that aiPI basin charges are slightly large and we should expect charges around 1.85 (Ca), 3.5 (Si), −1.75 (O), and 2.6 (B). These atomic charges are very important components in the development of force fields, that allow for a fast estimation of the lattice energy on geometries not far away from the static equilibrium arrangement.

TABLE 3: Volume and Charge of Ionic Basins in Danburite[a]

	V (Å^3)	Q (*e*)	*R* (Å)	⟨*R*⟩ (Å)
Ca	12.183	+1.921	1.427	1.213
B	0.717	+2.874	0.555	0.483
Si	2.388	+3.735	0.829	0.681
O1	14.910	−1.890	1.527	1.173
O2	14.387	−1.896	1.509	1.246
O3	13.738	−1.900	1.486	1.190
O4	17.225	−1.862	1.602	1.264
O5	14.599	−1.909	1.516	1.234

[a] Shown as a comparison, *R* is the radius of a sphere with the same volume as that of the basin, and ⟨*R*⟩ is the average of the topological radii.

Basin volumes, on the other hand, show the trends that should be expected from the atomic number and oxidation state of the ions: $\mathcal{V}_{O^{2-}} > \mathcal{V}_{Ca^{2+}} \gg \mathcal{V}_{Si^{4+}} > \mathcal{V}_{B^{3+}}$. The large variation among the volumes of oxide basins, from 13.7 Å^3 on O3 to 17.2 Å^3 on O4 is a little surprising. This variability is related to the role that anions play on filling the space in the crystal. This large difference in the O^{2-} basin volumes is not, however, accompanied by an equivalent variability in the ion charge, and we can conclude that the additional volume on some basins corresponds to very low-density regions. This is, probably, the reason for the rough correlation between basin volumes and average topological radii in danburite.

Once obtained, it is worth considering how the topological charges on the basins can be used. First of all, the charges provide a description, albeit a very limited one, of the distribution of electron density among the nuclei. It is possible, in principle, for two different electron densities to give equivalent descriptions of the critical points number and properties. The charges integrated over the basins give a different kind of information to distinguish them.

Furthermore, we can define an ionicity scale from the charges. We can compare, for instance, the topological charge, $\mathcal{Q}_i$, and the nominal oxidation state of an atom, Q_i, and define the *charge-transfer index*[80] of the atom in the crystal as

$$\mathcal{C}_i = 1 - \frac{Q_i - \mathcal{Q}_i}{Q_i} = \frac{\mathcal{Q}_i}{Q_i} \tag{3}$$

We have found, in all the crystals studied, that $|\mathcal{Q}_i| < |Q_i|$. The $\mathcal{C}_i$ are then positive and lie in the range [0, 1]. The charge-transfer index of the crystal, $\mathcal{C}$, can be obtained as an average of the atomic values. On a binary compound, A_mB_n, the cell neutrality condition determines that $\mathcal{C}_A = \mathcal{C}_B = \mathcal{C}$. In the case of danburite, the $\mathcal{C}_i$ values range from 0.931 in O4 to 0.961 in Ca, with an average value of 94.7% for the whole crystal. This value is similar to those found in the alkali halides or simple

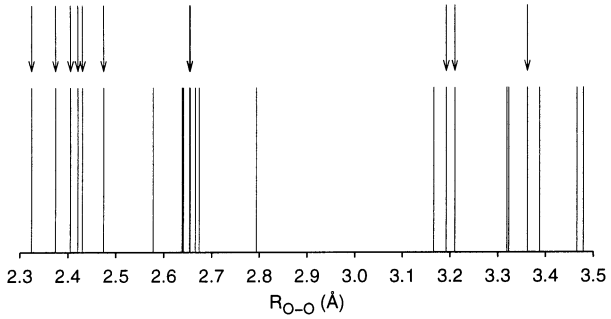

Figure 3. Plot of the shortest O−O distances in danburite. The actual topological bonds are indicated by arrows.

oxides.[30] As a general rule, the charge-transfer indexes defined in eq 3 are usually bigger than the ionicities obtained from Pauling's electronegativities.

V. Long-Distance O−O Bonds

We have already shown the existence of topological oide−oxide bond paths in danburite in addition to the typical metal−oxide bonds. We analyze now this evidence in detail and address the more general question of secondary (i.e. between second and further nearest neighbors) anion−anion bonds in crystals.

The occurrence of anion−anion bonds in ionic crystals has already been proposed several times: (a) Pauling discussed the importance of anion−anion contact in lithium halides.[79] He saw in this interaction the source of an additional repulsion, given the energy required to deform the anionic density. (b) O'Keefe and Brese[81] proposed a set of empirical rules to identify X−X bonds, where X is any of F^-, Cl^-, Br^-, I^-, O^{2-}, S^{2-}, and so forth. (c) Göttlicher and Vegas[82] observed the existence of O−O *density bridges* in a very high-quality X-ray determination of magnesite ($MgCO_3$), although later experiments on the same crystal by Maslen et al.[83] did not reproduce this observation. (d) The topological features of anion−anion bond critical points were already detected in many historical high-quality measurements of the total electron density like those of Krug et al.[84] on LiF, Göttlicher[85] on NaCl, and Niederauer and Göttlicher[86] on MgF_2, to name just a few.

Traditionally, O−O bonds have been described in a variety of forms: dioxygenil ion, O_2^+, as in O_2PtF_6;[87] neutral O_2 (ref 88) and O_3; ozonides containing the O_3^- group, like NH_4O_3;[89] superoxides containing the O_2^- group, like α-KO_2;[90] and peroxides having the O_2^{2-} group, like CdO_2 (ref 91) and H_2O_2.[92] The O−O distances in these molecular and crystalline compounds range from 1.1 to 1.5 Å.[93] The oide−oxide bond, on the other hand, would be described as an O_2^{4-} embedded group, and its O−O bond length would be 3.02 Å in $MgCO_3$ (ref 82) or 2.3−3.4 Å for the different O−O topological bonds in danburite.

Let us analyze the situation in danburite. Our topological analysis of the electron density indicates the existence of 11 different types of oxide−oxide bond critical points, with O−O bond lengths from 2.32 to 3.36 Å. The occurrence and spatial organization of oide−oxide bond paths in danburite are shown in Figures 3 and 4. Figure 3 clearly shows that bond critical points do not simply appear when the O−O distance is below some threshold. Together, both figures indicate that bond formation is a consequence of the local geometry of the ions basins or, in other words, it is due to the competition among neighboring ions to attract electrons. The case of O4 is, again, the best example of what can happen in extreme cases. Effectively, O4, the bridge atom between two SiO_4^{4-} tetrahedra

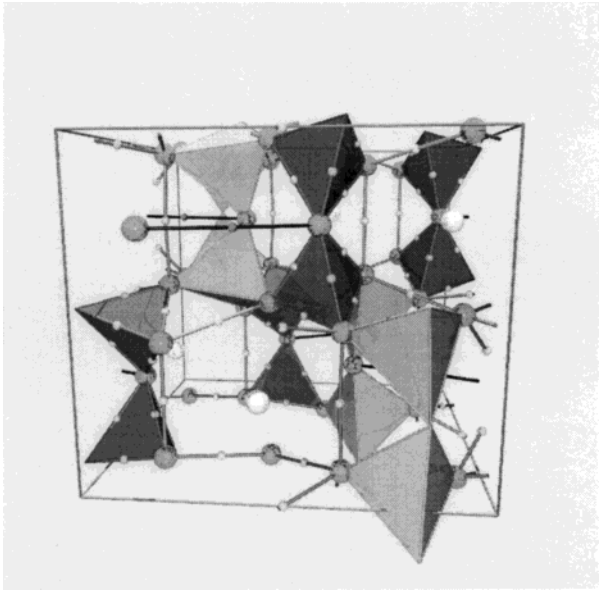

Figure 4. Molecular graph of danburite illustrating the position of the O−O bond critical points (small spheres) and the O−O bond paths (sticks passing through the bond critical point). The dark tetrahedra correspond to the B coordination polyhedra, and the light ones are the Si coordination polyhedra. The plot has been designed with Tessel[94] and rendered with POVRay.[95]

(see Figure 2), is not bonded to its six O^{2-} neighbors in the tetrahedra, but it is bonded to its ninth neighboring shell: an O5 situated 3.362 Å away.

The different behavior of SiO_4^{4-} and BO_4^{5-} coordination tetrahedra is worth noticing. Whereas the oxide ions in the BO_4^{5-} tetrahedra are bonded together, those in SiO_4^{4-} are not. If we assume a regular tetrahedron and consider the ions as rigid spheres, the anion−anion contact on the edges would happen only if the cation to anion radii ratio is $r_c/r_a \leq 1/\sqrt{2} \approx 0.707$. Using the average topological radii along the B−O and Si−O bonds, we find $r_B/r_O = 0.489$ and $r_{Si}/r_O = 0.727$. Thus, a simple rigid ion argument correctly predicts the existence of O−O bond paths on the BO_4^{5-} tetrahedra and their absence on the SiO_4^{4-} tetrahedra.

There is evidence supporting the suggestion that the O−O bond paths are not a quirk in the aiPI wave function. As we have remarked before, both aiPI and CRYSTAL98 agree on the prediction of O−O bonding in a collection of representative oxide crystals. For instance, according to both techniques, they will be present in MgO but not in CaO due to the different cation-to-anion ratio size.[30] The aiPI to CRYSTAL98 ρ_b(O−O) ratio varies between 60% and 130% for the representative set of crystals already cited. This may amount to a significative difference, but it must be taken into account that the Gaussian bases used on the CRYSTAL98 calculations are commonly not saturated and are optimized differently for each crystal instead. This produces a nonnegligible error bar on the low-density regions that varies from one crystal to another. We need, accordingly, a different test of the O−O density trends.

We have already seen, in the case of M−O bonding, that the bond properties of small molecules, when extrapolated to the distances found in crystals, can serve as a valid reference for the crystalline regime. We will try this strategy again to further analyze O−O bond critical points. Several reference molecules have, consequently, been selected: O_2, O_3, H_2O_2, O_2F_2, and the planar and nonplanar configurations of $C(NO_2)_3^-$. Hartree−Fock (HF) calculations have been done at the theoretical ($C(NO_2)_3^-$) or experimental (the rest of molecules) equilibrium

TABLE 4: Topological Properties of O−O Bond Critical Points in a Collection of Crystals and Gas Phase Molecules[a]

system	d_{OO}	ρ_b	$\nabla^2\rho_b$	$\lambda_3(b)$	ϵ	O−b−O
α-Al_2O_3 (ref 99)	2.361	0.282 22	4.827 71	7.207 22	1.79	179.56
	2.464	0.216 08	3.890 50	5.621 76	4.27	180.00
	2.606	0.149 88	2.879 32	3.969 31	5.97	178.54
BaO (ref 100)	(3.917)					
CaO (ref 100)	(3.402)					
$CaTiO_3$ (*Cmmm*) (ref 101)	(3.273)					
$CaTiO_3$ (*Pbnm*) (ref 101)	3.350	0.025 10	0.566 32	0.611 87	71.51	180.00
$CaTiO_3$ (*Pm*3*m*) (ref 99)	(2.715)					
danburite (ref 14)	2.325	0.312 72	5.047 25	7.668 95	3.35	179.38
	2.374	0.276 61	4.568 88	6.797 06	6.19	178.98
	2.405	0.255 36	4.366 46	6.321 11	15.09	178.72
	2.420	0.245 50	4.225 24	6.101 81	13.11	178.41
	2.430	0.239 57	4.142 10	5.956 01	12.06	178.31
	2.474	0.217 16	3.956 29	5.293 05	44.55	176.29
	2.655	0.133 62	2.489 64	3.453 35	12.13	178.21
	2.793	0.093 73	1.798 97	2.452 53	10.33	179.15
	3.192	0.033 27	0.707 30	0.910 93	3.52	180.00
	3.210	0.033 61	0.737 90	0.852 61	88.98	175.45
	3.831	0.006 48	0.156 40	0.172 55	4.96	173.70
Li_2O (ref 100)	(3.266)					
MgO (ref 100)	2.977	0.072 88	1.220 60	1.616 06	21.48	180.00
SiO_2 (tridymite) (ref 101)	(2.515)					
SiO_2 (α-cristobalite) (ref 99)	3.962	0.004 18	0.103 38	0.120 98	45.78	177.36
SiO_2 (α-quartz) (ref 99)	3.299	0.024 90	0.531 86	0.683 68	5.17	179.84
	3.563	0.012 42	0.280 51	0.346 30	2.34	179.30
	3.578	0.012 21	0.278 34	0.331 36	21.81	176.71
SiO_2 (β-cristobalite) (ref 99)	(2.616)					
SiO_2 (β-quartz) (ref 99)	3.420	0.018 56	0.403 90	0.504 63	5.61	180.00
	3.477	0.015 86	0.349 43	0.433 78	2.02	178.14
SrO (ref 100)	(3.649)					
TiO_2 (anatase) (ref 99)	1.892	0.701 15	15.743 48	24.937 40	0.27	179.95
	2.050	0.439 32	11.974 92	16.368 36	33.40	179.56
	3.473	0.007 56	0.012 53	0.025 06	0.00	137.85
TiO_2 (rutile) (ref 102)	2.536	0.179 30	3.508 06	4.671 55	43.41	180.00
	3.325	0.021 66	0.537 88	0.625 60	14.78	180.00
ZnO (ref 103)	(3.209)					
ZrO_2 (cubic) (ref 100)	2.545	0.182 07	3.251 65	4.606 48	15.29	180.00
O_2(g)	1.208	3.635 13	−22.084 44	47.080 56	0.00	180.00
F_2O_2(g)	1.217	3.603 53	−24.455 09	47.624 89	0.72	
O_3(g)	1.278	2.969 36	−8.975 05	29.353 37	11.10	
H_2O_2(g)	1.452	1.917 04	−2.758 18	27.679 77	5.25	
$C(NO_2)_3^-$(planar)	2.453	0.171 65	3.226 75	4.654 89	12.07	
$C(NO_2)_3^-$(nonplanar)	2.689	0.101 26	1.913 29	2.423 46	39.02	

[a] Crystal calculations have been done with the aiPI method at the experimental geometries, using a large STO basis set. Molecular calculations have been done at the experimental geometry using a HF/TZV+(3d) method, except for the trinitromethynide ion, for which the geometry has been optimized at the HF/TZV+(1d) level using both a D_{3h} (planar) and a D_3 (nonplanar) configuration. Distances (d_{OO}) are given in Å, bond densities (ρ_b) in e/Å^3, bond Laplacians and curvatures ($\nabla^2\rho_b$ and $\lambda_3(b)$) in e/Å^5, ellipticities in %, and angles in deg. In those crystals where there is no O−O bond, d_{OO} corresponds to the shortest O−O distance.

geometries. In the case of O_2, we have done HF calculations on the $^3\Sigma_g^-$ ground state from 0.8 to 4.2 Å, taking great care to keep the same electronic state at all distances. The effect of basis sets has been analyzed extensively, but only the best results using a TZV+(3d) basis consisting of a triple-ζ valence,[75,96] diffuse sp functions,[97] and three d polarization functions[98] will be discussed here (a TZV+(1d) basis set in the case of $C(NO_2)_3^-$). Correlation effects, up to a CI-SD level, were found to have a negligible influence on the topology of the electron density of O_2.

The O−O bond properties calculated on a collection of crystals and gas phase molecules are presented in Table 4. The results shown there clearly indicate that the occurrence of O−O bond critical points is not uniquely due to the O−O distance. The trinitromethanyde ion, $C(NO_2)_3^-$, provides a clear illustration of this point. The shortest O−O distance is 2.084 Å between the two oxygens in a NO_2 group, but there is no bond path among them. The electron density gradient vector field of the molecule, depicted in Figure 5, shows how each N basin interposes as a barrier between the two oxygens in its NO_2 group, preventing the existence of a bond path among them. The oxygens in different NO_2 groups, however, have no such limitation, and even though their distance (2.453 Å) is larger than that within a NO_2 group, the molecule presents three O−O bonds. Similarly, the topological analysis of simple and highly symmetric crystalline structures has made it clear that the occurrence of secondary anion−anion bond critical points (or cation−cation bonds in some cases) is regulated by the ratio of topological radii along the main cation−anion bond paths.[11,46,47] The analysis of low symmetry crystals or molecules is more difficult, but the same principles should apply, and we could say that the occurrence of secondary bonds between two atoms is controlled not by the distance but rather by the size of the nearest neighbors' basins around both atoms.

On the other hand, the electron density at the O−O bond critical point decays exponentially with the O−O distance, as we can see in Figure 6. This behavior is closely followed by molecules and crystals, for distances from 1.2 to 3.2 Å, and for bonds whose densities range from 5 to 0.005 e/Å^3. As we had expected, the behavior of the bond in the O_2 molecule with the

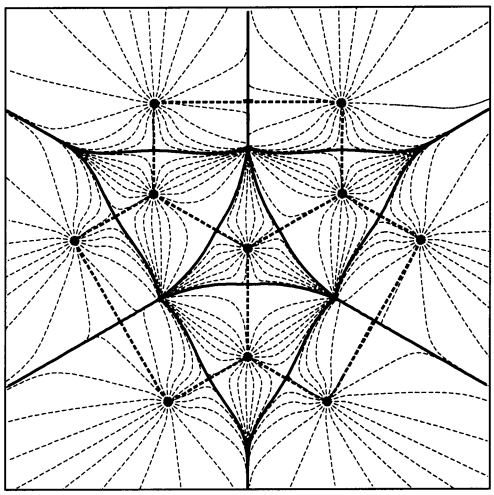

Figure 5. Electron density gradient vector field of $C(NO_2)_3^-$ at the optimal HF/TZV+(1d) planar geometry. In addition to the expected C−N and N−O bond critical points, the molecule presents O−O bonds connecting neighbor NO_2 groups, and ring points within each ONCNO pentagon. It is readily seen that O−O bonds occur only between NO_2 groups, as the N basin extends through the two oxygens in each NO_2 group. The topology of the nonplanar optimal configuration is identical, albeit less simple to visualize.

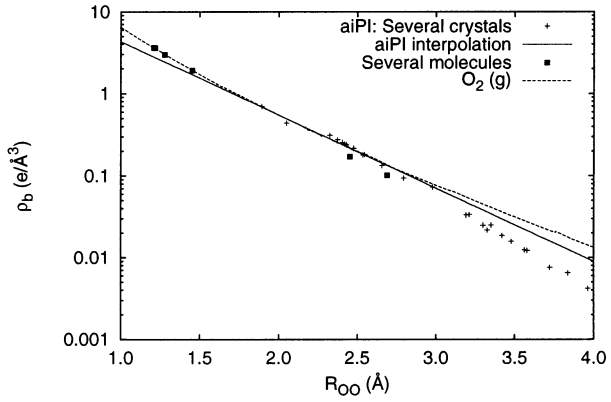

Figure 6. Electron density at the O−O bonds, in a collection of molecules and crystals, represented against the O−O distance. The electron density for the O_2 molecule has been obtained on a wide range of distances rather than at a single geometry, like in the case of the other systems. The ρ_b value for the crystals has been represented by the best fit exponential law, $\rho_b(r_{OO}) = A \exp(-\alpha r_{OO})$, where $A = 33.692$ e/Å^3 and $\alpha = 2.0569$ Å^{-1}. Notice the logarithmic scale used on the vertical axis.

distance passes through the actual values of the other molecules and crystals, therefore representing an appropriate model for the O−O bond.

The O_2 molecule also provides an appropriate model for the Laplacian of the electron density at the O−O bond critical point, although it is less precise than in the case of the bond density. We can observe in Figure 7 that the bond character changes from mainly covalent ($\nabla^2\rho_b < 0$) to mainly closed-shell-like ($\nabla^2\rho_b > 0$) as the O−O distance passes from below to above 1.5 Å, respectively. Accordingly, the O−O bond is clearly ionic (or closed-shell) in most crystals, whereas it can be either covalent or ionic in the molecules.

The above results show, in our opinion, a clear evidence in favor of the real occurrence of O−O secondary bonds in many crystals, and they also show the continuity in the bond properties of the O−O dumbbell from the molecular to the crystal regime, the internuclear distance being the main control parameter.

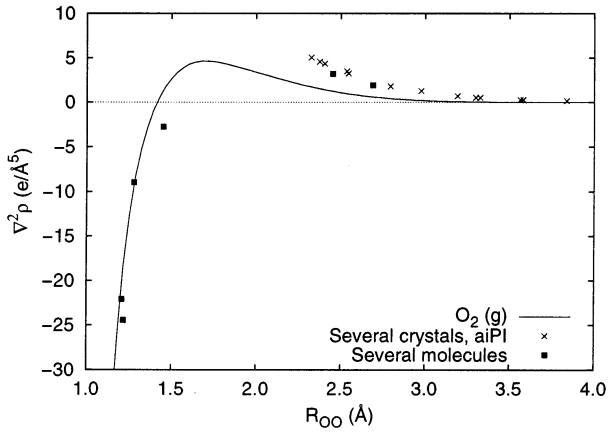

Figure 7. Laplacian of ρ_b(O−O) for a collection of molecules and crystals. The value of $\nabla^2\rho_b$ of the O_2 molecule has been obtained in a range of internuclear distances, and it provides an approximate model for all the compounds.

Several authors, on the other hand, have raised legitimate concerns about the physical meaning of anion−anion bonding in crystals,[59] "sterically interacting" atoms[57] or long-distance nonclassical bonds in general.[55,56,104]

Abramov,[59] for instance, based his main argument on a particular decomposition of the lattice energy into Coulombic and short-range repulsive terms by using Bader's basin charges within a simple electrostatic formula that assumes pointlike ions. According to this partitioning scheme, the anion−anion interactions (or the cation−cation ones) could only destabilize the crystal by raising the Coulomb energy. It must be noticed, however, that atomic basins are far from being spherical and pointlike and that quite important multipolar interactions do exist, as has been demonstrated by Popelier.[105,106] A thorough analysis of whether the local distribution of electron density of the anion−anion interaction line represents a bonding or antibonding net contribution in the energetic sense could be done using Berlin's methods.[107] Such analysis has been used extensively, to the best of our knowledge, only on simple diatomic molecules,[108−112] and its generalization to more complex molecules and even crystals could be described as a nightmare (see, however, ref 113).

Cioslowski et al.[55−57,104] have tried to classify long-distance, weak topological bonds into true chemical bonds (like those appearing in van der Waals interactions[114] and hydrogen bridges,[115,116] for instance) and interactions appearing only for "steric reasons". The O−O bond in the planar configuration of the trinitromethanyde ion, $C(NO_2)_3^-$, is proposed as a typical example of a molecule with steric interactions.[57] It could be argued, however, that the "steric crowding" is eliminated in the nonplanar optimal geometry of $C(NO_2)_3^-$ by the rotation of the NO_2 groups around the C−N axes, but the fact is that the O−O bonds do not disappear by this relaxation of the symmetry (see Table 4). In addition, as we have shown previously, the topological properties of O−O bond paths display a clear continuity from their occurrence as *strong bonds* in many molecules to the *weak* second and longer range interactions appearing in many crystal oxides, the *effective bond order* being determined by the O−O distance.

More fundamentally, the occurrence of closed-shell weak bonds in molecules and crystals has been discussed by Bader.[117] After examining the atomic and local theorems governing atomic interactions, Bader concludes that the presence of a (3, −1) critical point of the electron density and its associated atomic interaction line in a stationary state of a molecule or crystal is

both necessary and sufficient for the two atoms to be bonded to one another in the usual chemical sense of the word. In addition, "there are no repulsive contributions to the total potential energy locally nor from atoms or ions within a system" and "only an excess electronic kinetic energy can lead to repulsions within the system", the electronic potential energy being always stabilizing.[117] Finally, even though the Lewis model of bonding in terms of the formation of one pair of electrons per bond is clearly unable to deal with bonding in closed-shell systems, this idea can be generalized to include less than complete pairing. Accordingly, closed-shell interactions (either weak or strong) and shared interactions are, both, due to the pairing of the densities of opposite spin electrons.

VI. Conclusions

To conclude, we want to stress the usefulness of comparing high-quality electron densities from experiments and theoretical calculations to further improve our knowledge of chemical bonding in light of the new paradigm provided by the atoms in molecules theory. A universal indication of a bonding interaction between two atoms, for short as well as long distances, is the occurrence of a bond critical point and its associated bond path connecting both atoms. The extrapolation of bond properties from small molecules to the solid-state regime appears as a promising auxiliary technique that should be further explored.

Acknowledgment. We are grateful to the Spanish DGICyT, Grant BQU2000-0466, for financial support. A.C. thanks the Ministerio de Ciencia y Tecnología for her Ramón y Cajal fellowship. P.M.S. is now a Fulbright fellow at Duke University. Careful reading of the manuscript by L. Pueyo is gratefully acknowledged.

References and Notes

(1) Bader, R. F. W. *Acc. Chem. Res.* **1975**, *8*, 34−40.
(2) Srebrenik, S.; Bader, R. F. W.; Nguyen-Dang, T. T. *J. Chem. Phys.* **1978**, *68*, 3667−3679.
(3) Bader, R. F. W.; Nguyen-Dang, T. T. *Adv. Quantum Chem.* **1981**, *14*, 63−124.
(4) Bader, R. F. W. *Atoms in Molecules. A Quantum Theory*; Oxford University Press: Oxford, U.K., 1990.
(5) Bader, R. F. W.; Popelier, P. L. A.; Keith, T. A. *Angew. Chem., Int. Ed. Engl.* **1994**, *33*, 620−631.
(6) Bader, R. F. W. *Phys. Rev. B* **1994**, *49*, 13348−13356.
(7) Feynman, R. P. *Rev. Mod. Phys.* **1948**, *20*, 367−387.
(8) Schwinger, J. *Phys. Rev.* **1951**, *82*, 914−927.
(9) Zou, P. F.; Bader, R. F. W. *Acta Crystallogr., A* **1994**, *50*, 714−725.
(10) Tsirelson, V. G.; Zou, P. F.; Tang, T. H.; Bader, R. F. W. *Acta Crystallogr., A* **1995**, *51*, 143−153.
(11) Pendás, A. M.; Costales, A.; Luaña, V. *Phys. Rev. B* **1997**, *55*, 4275−4284.
(12) Fujino, K.; Sasaki, S.; Takéuchi, Y.; Sadanaga, R. *Acta Crystallogr., B* **1981**, *37*, 513−518.
(13) Spackman, M. A.; Gibbs, G. V.; Hill, R. J. *Phys. Chem. Miner.* **1987**, *14*, 139−150.
(14) Downs, J. W.; Swope, R. J. *J. Phys. Chem.* **1992**, *96*, 4834−4840.
(15) Downs, R. T.; Andalman, A.; Hudacsko, M. *Am. Mineral.* **1996**, *81*, 1344−1349.
(16) Ghermani, N. E.; Lecomte, C.; Dusausoy, Y. *Phys. Rev. B* **1996**, *53*, 5231−5239.
(17) Hénaff, C. L.; Hansen, N. K.; Protas, J.; Marnier, G. *Acta Crystallogr., B* **1997**, *53*, 870−879.
(18) Ivanov, Y. V.; Belokoneva, E. L.; Protas, J.; Hansen, N. K.; Tsirelson, V. G. *Acta Crystallogr., B* **1998**, *54*, 774−781.
(19) Koritsanszky, T. S.; Coppens, P. *Chem. Rev.* **2001**, *101*, 1583−1627.
(20) Downs, R. T.; Gibbs, G. V.; Boisen, M. B., Jr.; Rosso, K. M. *Phys. Chem. Miner.* **2002**, *29*, 369−385.
(21) Abramov, Y. A.; Okamura, F. P. *Acta Crystallogr., A* **1997**, *53*, 187−198.
(22) Takata, M.; Sakata, M.; Kumazawa, S.; Larsen, F. K.; Iversen, B. B. *Acta Crystallogr., A* **1994**, *50*, 330−337.
(23) Kappkhan, M.; Ozerov, R. P.; Tsirelson, V. G. *Dokl. Akad. Nauk* **1988**, *303*, 404−408.
(24) Wiberg, K. B.; Waldron, R. F.; Schulte, G.; Saunders, M. *J. Am. Chem. Soc.* **1991**, *113*, 971−977.
(25) Vyboishchikov, S. F.; Masunov, A. E.; Streltsov, V. A.; Zorkii, P. M.; Tsirelson, V. G. *Zh. Fiz. Khim.* **1994**, *68*, 2024−2028.
(26) Boese, R.; Boese, A. D.; Blaser, D.; Antipin, M. Y.; Ellern, A.; Seppelt, K. *Angew. Chem., Int. Ed. Engl.* **1997**, *36*, 1489−1492.
(27) Boese, R.; Niederprum, N.; Blaser, D.; Maulitz, A.; Antipin, M. Y.; Mallinson, P. R. *J. Phys. Chem. B* **1997**, *101*, 5794−5799.
(28) Mei, C. J.; Edgecombe, K. E.; Smith, V. H.; Heilingbrunner, A. *Int. J. Quantum Chem.* **1993**, *48*, 287−293.
(29) Aray, Y.; Rodriguez, J.; Lopez-Boada, R. *J. Phys. Chem. A* **1997**, *101*, 2178−2184.
(30) Mori-Sánchez, P. Densidad electrónica y enlace químico. De la molécula al cristal. Ph.D. Thesis, Universidad de Oviedo, 2002. See http://www.uniovi.es/~quimica.fisica/qcg/pms/tesis.html.
(31) Eberhart, M. E.; Clougherty, D. P.; MacLaren, J. M. *Philos. Mag. B* **1993**, *68*, 455−464.
(32) Eberhart, M. E.; Clougherty, D. P.; MacLaren, J. M. *J. Am. Chem. Soc.* **1993**, *115*, 5762−5767.
(33) Eberhart, M. E.; Clougherty, D. P.; MacLaren, J. M. *J. Mater. Res.* **1993**, *8*, 438−448.
(34) Haussermann, U.; Wengert, S.; Hofmann, P.; Savin, A.; Jepsen, O.; Nesper, R. *Angew. Chem., Int. Ed. Engl.* **1994**, *33*, 2069−2073.
(35) Haussermann, U.; Wengert, S.; Nesper, R. *Angew. Chem., Int. Ed. Engl.* **1994**, *33*, 2073−2076.
(36) Grosch, G. H.; Freytag, B.; Range, K. J.; Rossler, U. *J. Chem. Phys.* **1994**, *101*, 6782−6789.
(37) Grosch, G. H.; Range, K. J. *J. Alloys Compd.* **1996**, *235*, 250−255.
(38) Grosch, G. H.; Range, K. J. *J. Alloys Compd.* **1996**, *233*, 30−38.
(39) Grosch, G. H.; Range, K. J. *J. Alloys Compd.* **1996**, *233*, 39−43.
(40) Knecht, M.; Ebert, H.; Bensch, W. *J. Alloys Compd.* **1997**, *246*, 166−176.
(41) Gatti, C.; Saunders, V. R.; Roetti, C. *J. Chem. Phys.* **1994**, *101*, 10686−10696.
(42) Platts, J. A.; Howard, S. T. *J. Chem. Phys.* **1996**, *105*, 4668−4674.
(43) Asthalter, T.; Weyrich, W. *Ber. Bunsen-Ges. Phys. Chem.* **1992**, *96*, 1747−1755.
(44) Fahmi, A.; Minot, C.; Silvi, B.; Causa, M. *Phys. Rev. B* **1993**, *47*, 11717−11724.
(45) Hahn, U.; Weber, W. *Phys. Rev. B* **1996**, *53*, 12684−12693.
(46) Luaña, V.; Costales, A.; Pendás, A. M. *Phys. Rev. B* **1997**, *55*, 4285−4297.
(47) Pendás, A. M.; Costales, A.; Luaña, V. *J. Phys. Chem. B* **1998**, *102*, 6937−6948.
(48) Blanco, M. A.; Costales, A.; Pendás, A. M.; Luaña, V. *Phys. Rev. B* **2000**, *62*, 12028−12039.
(49) Costales Castro, A. Topología de la densidad electrónica en cristales. Una teoría cuántica del enlace cristalino. Ph.D. Thesis, Universidad de Oviedo, 1998. See http://www.uniovi.es/~quimica.fisica/qcg/acc/tesis.html.
(50) Pierloot, K.; Vanpraet, E.; Vanquickenborne, L. G. *J. Chem. Phys.* **1995**, *102*, 1164−1172.
(51) Bader, R. F. W.; Platts, J. A. *J. Chem. Phys.* **1997**, *107*, 8545−8553.
(52) Cargnoni, F.; Colombo, L.; Gatti, C. *Nucl. Instrum. Methods Phys. Res., Sect. B* **1997**, *127*, 235−238.
(53) Mori-Sánchez, P.; Recio, J. M.; Silvi, B.; Sousa, C.; Pendás, A. M.; Luaña, V.; Illas, F. *Phys. Rev. B* **2002**, *66*, 075103−1−6.
(54) Feth, S.; Gibbs, G. V.; Boisen, M. B.; Myers, R. H. *J. Phys. Chem.* **1993**, *97*, 11445−11450.
(55) Cioslowski, J.; Mixon, S. T.; Edwards, W. D. *J. Am. Chem. Soc.* **1991**, *113*, 1083−1085.
(56) Cioslowski, J.; Mixon, S. T. *J. Am. Chem. Soc.* **1992**, *114*, 4382−4387.
(57) Cioslowski, J.; Edgington, L.; Stefanov, B. B. *J. Am. Chem. Soc.* **1995**, *117*, 10381−10384.
(58) Browning, C. S.; Burrow, T. E.; Farrar, D. H.; Lough, A. J. *Acta Crystallogr., C* **1996**, *52*, 652−654.
(59) Abramov, Y. A. *J. Phys. Chem. A* **1997**, *101*, 5725−5728.
(60) Luaña, V.; Pueyo, L. *Phys. Rev. B* **1990**, *41*, 3800−3814.
(61) Luaña, V.; Pendás, A. M.; Recio, J. M.; Francisco, E.; Bermejo, M. *Comput. Phys. Commun.* **1993**, *77*, 107−134.
(62) Blanco, M. A.; Luaña, V.; Pendás, A. M. *Comput. Phys. Commun.* **1997**, *103*, 287−302.
(63) Luaña, V.; Pueyo, L. *Phys. Rev. B* **1989**, *39*, 11093−11112.
(64) Francisco, E.; Pendás, A. M.; Adams, W. H. *J. Chem. Phys.* **1992**, *97*, 6504−6508.
(65) Luaña, V.; Recio, J. M.; Pueyo, L. *Phys. Rev. B* **1990**, *42*, 1791−1801.

(66) Luaña, V.; Flórez, M.; Pueyo, L. *J. Chem. Phys.* **1993**, *99*, 7970−7982.
(67) Recio, J. M.; Pandey, R.; Luaña, V. *Phys. Rev. B* **1993**, *47*, 3401−3403.
(68) Beltrán, A.; Flores Riveros, A.; Andrés, J.; Luaña, V.; Pendás, A. M. *J. Phys. Chem.* **1994**, *98*, 7741−7744.
(69) Pendás, A. M.; Luaña, V.; Recio, J. M.; Flórez, M.; Francisco, E.; Blanco, M. A.; Kantorovich, L. N. *Phys. Rev. B* **1994**, *49*, 3066−3074.
(70) Pendás, A. M.; Recio, J. M.; Flórez, M.; Luaña, V.; Bermejo, M. *Phys. Rev. B* **1994**, *49*, 5858−5868.
(71) Francisco, E.; Recio, J. M.; Blanco, M. A.; Pendás, A. M.; Costales, A. *J. Phys. Chem. A* **1998**, *102*, 1595−1601.
(72) Clementi, E.; Roetti, C. *At. Data Nucl. Data Tables* **1974**, *14*, 177.
(73) Dovesi, R.; Saunders, V. R.; Roetti, C.; Causà, M.; Harrison, N. M.; Orlando, R.; Zicovich-Wilson, C. M. *CRYSTAL98 User's Manual*; University of Torino, Italy, 1998.
(74) Pendás, A. M.; Luaña, V. *The critic program*; Universidad de Oviedo, Spain, 1995−2003.
(75) Schmidt, M. W.; Baldridge, K. K.; Boatz, J. A.; Elbert, S. T.; Gordon, M. S.; Jensen, J. H.; Koseki, S.; Matsunaga, N.; Nguyen, K. A.; Su, S. J.; Windus, T. L.; Dupuis, M.; Montgomery, J. A. *J. Comput. Chem.* **1993**, *14*, 1347−1363.
(76) R. W. F. Bader's Laboratory. *AIMPAC*; 1989. Available from http://www.chemistry.mcmaster.ca/aimpac/.
(77) Álvarez Blanco, M. Métodos cuánticos locales para la simulación de materiales iónicos. Fundamentos, algoritmos y aplicaciones. Ph.D. Thesis, Universidad de Oviedo, 1997. See http://www.uniovi.es/~quimica.fisica/qcg/mab/tesis.html.
(78) Phillips, M.; Munzner, T.; Levy, S. *Geomview*; The Geometry Center at the University of Minnesotta: 1995. Available from http://www.geomview.org.
(79) Pauling, L. *The nature of the chemical bond, and the structure of molecules and crystals*, 3rd ed.; Cornell University Press: Ithaca, NY, 1960.
(80) Mori-Sánchez, P.; Pendás, A. M.; Luaña, V. *J. Am. Chem. Soc.* **2002**, *124*, 14721−14723.
(81) O'Keefe, M.; Brese, N. E. *Acta Crystallogr., B* **1992**, *48*, 152.
(82) Göttlicher, S.; Vegas, A. *Acta Crystallogr., B* **1988**, *44*, 362−367.
(83) Maslen, E. N.; Streltsov, V. A.; Streltsova, N. R. *Acta Crystallogr., B* **1993**, *49*, 980−984.
(84) Krug, J.; White, H.; Wölfel, E. *Z. Phys. Chem.* **1955**, *4*, 36−64.
(85) Göttlicher, V. S. *Acta Crystallogr., B* **1968**, *24*, 122−129.
(86) Niederauer, K.; Göttlicher, S. *Z. Angew. Phys.* **1970**, *29*, 16−21.
(87) Ibers, J. A.; Hamilton, W. C. *J. Chem. Phys.* **1966**, *44*, 1748−1752.
(88) Miller, S. L.; Townes, C. H. *Phys. Rev.* **1953**, *90*, 537−543.
(89) Solomon, I. J.; Hattori, K.; Kacmarek, A. J.; Platz, G. M.; Klein, M. J. *J. Am. Chem. Soc.* **1962**, *84*, 34−36.
(90) Abrahams, S. J.; Kalnajs, J. *Acta Crystallogr.* **1955**, *8*, 503−506.
(91) Hoffman, C. W. W.; Ropp, R. C.; Mooney, R. W. *J. Am. Chem. Soc.* **1959**, *81*, 3830−3834.
(92) Redington, R. L.; Olson, W. B.; Cross, P. C. *J. Chem. Phys.* **1962**, *36*, 1311−1326.
(93) Wells, A. F. *Structural inorganic chemistry*; Oxford University Press: Oxford, U.K., 1987.
(94) Luaña, V. *Tessel version 2*; Universidad de Oviedo, Spain, 1997−2003. Available from http://www.uniovi.es/~quimica.fisica/qcg/src/tessel.html.
(95) Anger, S.; Bayer, D.; Cason, C.; Dailey, C.; Dilger, A.; Demlow, S.; Enzmann, A.; Wegner, D. F. T.; Young, C. *POV−Ray: Persistence of the Vision Ray Tracer*; 1997. Available from http://www.povray.org.
(96) Binning, R. C., Jr.; Curtiss, L. A. *J. Comput. Chem.* **1990**, *11*, 1206−1216.
(97) Clark, T.; Chandrasekhar, J.; Spitznagel, G. W.; Schleyer, P. v. R. *J. Comput. Chem.* **1983**, *4*, 294−301.
(98) Frisch, M. J.; Pople, J. A.; Binkley, J. S. *J. Chem. Phys.* **1984**, *80*, 3265−3269.
(99) Hyde, B. G.; Anderson, S. *Inorganic crystal structures*; Wiley: New York, 1989.
(100) Wyckoff, R. W. G. *Crystal structures*, Vol. 1; Interscience: New York, 1960.
(101) *Inorganic crystal structure database (ICSD)*; Karlsruhe, Germany, 1998.
(102) Abrahams, S. C.; Bernstein, J. L. *J. Chem. Phys.* **1971**, *55*, 3206.
(103) Abrahams, S. C.; Bernstein, J. L. *Acta Crystallogr., B* **1969**, *25*, 1233.
(104) Cioslowski, J.; Mixon, S. T. *Can. J. Chem.* **1992**, *70*, 443−449.
(105) Kosov, D. S.; Popelier, P. L. A. *J. Chem. Phys.* **2000**, *113*, 3969−3974.
(106) Kosov, D. S.; Popelier, P. L. A. *J. Phys. Chem. A* **2000**, *104*, 7339−7345.
(107) Berlin, T. *J. Chem. Phys.* **1951**, *19*, 208−213.
(108) Bader, R. F. W.; Henneker, W. H.; Cade, P. E. *J. Chem. Phys.* **1967**, *46*, 3341−3363.
(109) Bader, R. F. W.; Keaveny, I.; Cade, P. E. *J. Chem. Phys.* **1967**, *47*, 3381−3402.
(110) Bader, R. F. W.; Bandrauk, A. D. *J. Chem. Phys.* **1968**, *49*, 1653−1665.
(111) Cade, P. E.; Bader, R. F. W.; Henneker, W. H.; Keaveny, I. *J. Chem. Phys.* **1969**, *50*, 5313−5333.
(112) Cade, P. E.; Bader, R. F. W.; Pelletier, J. *J. Chem. Phys.* **1971**, *54*, 3517−3533.
(113) Koga, T.; Nakatsuji, H.; Yonezawa, T. *J. Am. Chem. Soc.* **1978**, *100*, 7522−7527.
(114) Bone, R. G. A.; Bader, R. F. W. *J. Phys. Chem.* **1996**, *100*, 10892−10911.
(115) Carroll, M. T.; Bader, R. F. W. *Mol. Phys.* **1988**, *65*, 695−722.
(116) Destro, R.; Bianchi, R.; Gatti, C.; Merati, F. *Chem. Phys. Lett.* **1991**, *186*, 47−52.
(117) Bader, R. F. W. *J. Phys. Chem. A* **1998**, *102*, 7314−7323.